# ChemComm

Accepted Manuscript


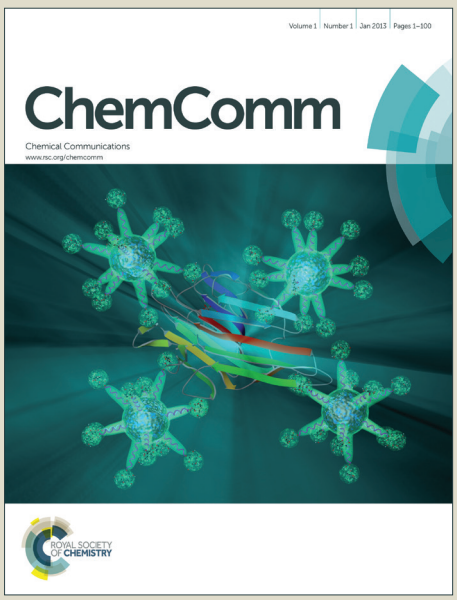



This is an *Accepted Manuscript*, which has been through the Royal Society of Chemistry peer review process and has been accepted for publication.

*Accepted Manuscripts* are published online shortly after acceptance, before technical editing, formatting and proof reading. Using this free service, authors can make their results available to the community, in citable form, before we publish the edited article. We will replace this *Accepted Manuscript* with the edited and formatted *Advance Article* as soon as it is available.

You can find more information about *Accepted Manuscripts* in the Information for Authors.

Please note that technical editing may introduce minor changes to the text and/or graphics, which may alter content. The journal's standard Terms & Conditions and the Ethical guidelines still apply. In no event shall the Royal Society of Chemistry be held responsible for any errors or omissions in this *Accepted Manuscript* or any consequences arising from the use of any information it contains.



ROYAL SOCIETY OF CHEMISTRY

www.rsc.org/chemcomm

Please do not adjust margins

Journal Name

COMMUNICATION

# Self-Assembled NIR Nanovesicles for Long-Term Photoacoustic Imaging *In Vivo*

Received 00th January 20xx,
Accepted 00th January 20xx

DOI: 10.1039/x0xx00000x

www.rsc.org/

Hong-Wei An,[a,b] Sheng-Lin Qiao,[a,b] Chun-Yuan Hou,[a] Yao-Xin Lin,[a,b] Li-Li Li,[a] Han-Yi Xie,[a] Yi Wang,[a,b] Lei Wang*,[a] and Hao Wang*,[a]

**We report a supramolecular approach for preparation of photostable NIR nanovesicles based on a cyanine dye derivative as a photoacoustic (PA) contrast agent for high-performance nano-imaging.**

Supramolecular nanostructures have emerged as promising materials for bioimaging.[1] A variety of building blocks such as π-conjugated dyes,[2] ionic oligomers,[3] amphiphilic polymers,[4] and metal complexes[5], *etc.* were utilized for constructing functional supramolecular contrast agents.[6] The resulting self-assembled nano-sized superstructures show enhanced tumor sensitivity and specificity due to their increased accumulation in tumor site by EPR effect.[7] Long-term imaging gains increasing attentions owing to its widely applications in biology[8] and medicine.[9] Photoacoustic tomography (PAT, also called optoacoustic tomography) is a non-invasive bioimaging technique that can generate real-time, high-resolution and 3D reconstructive images.[10] PAT contrast agents include inorganic materials (*e.g.* carbon nanostructure,[11] quantum dots[12] and gold nanoparticles[13]), polymers (*e.g.* dendrimers[14] and semiconducting polymers[10c]) and organic molecules (*e.g.* cyanine dyes,[15] squaraine dyes,[16] anthocyanin dyes[17] and porphyrins[18]). So far, indocyanine green (ICG) was the only FDA approved contrast agent outlined above. However, the poor photo and chemical stabilities greatly hamper their utilization in fundamental researches as well as clinic practices.[19] In some cases, the pharmacokinetics, biodistribution and metabolism studies are required for quantitatively determining physiological parameters of drug/contrast agents *in vivo*,[20] as well as guiding significance to clinical diagnosis and treatment. The structural modification[19b, 21] or physical doping[19a, 22] approaches have been exploited for augmenting its stability. Recently, our group has been focused on the construction of organic dye aggregates-based nanosystems for bioimaging.[2e, 23] We have developed the *J*-type bis(pyrene) nanoparticles for cellular imaging.[24] More recently, we found that the supramolecular strategy enable modulating squaraine dye's optical property and stability to achieve high-performance bioimaging.[2e]

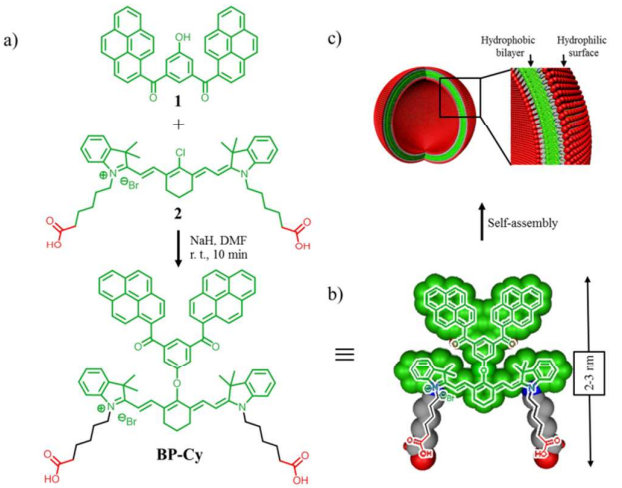


**Scheme 1**. Self-assembly of the bis-pyrene conjugated cyanine dye (**BP-Cy**) into a vesicular nanoaggregates. a) Molecular structures of **1**, **2**, **BP-Cy**. b) The schematic representation of **BP-Cy** and c) the self-assembled vesicular nanoaggregate of **BP-Cy**.

Herein, we introduced a bis(pyrene)-extended conjugated cyanine dye (**BP-Cy**) for constructing a well-organized NIR absorbing nanovesicles with superb chemical and photostability (Scheme 1). Owing to the intrinsic structural characteristic, the cyanine dyes preferentially self-assembled into lamellar or tubular superstructures.[25] We tailored the π-scaffolds of cyanine dyes and firstly reported their vesicular self-assembly without templates, to the best of our knowledge.[26] Interestingly, compared with the monomer and analogue ICG molecules, the stable nanovesicles show significantly improved PA signal intensity and half-life *in vitro* and *in vivo*.

The hydrophobic unit bis(pyrene) **1** and NIR absorbable cyanine **2** were synthesized in our lab (See Supporting Information).

[a] *CAS Key Laboratory for Biological Effects of Nanomaterials and Nanosafety, National Center for Nanoscience and Technology (NCNST), No. 11 Beiyitiao, Zhongguancun, Beijing, China. E-mail: wanghao@nanoctr.cn*
[b] *University of Chinese Academy of Science (UCAS), No. 19A Yuquan Road, Beijing, China*

† Electronic Supplementary Information (ESI) available: Experimental details; Scheme 1; Table S1; and Fig S1-S12. See DOI: 10.1039/x0xx00000x

ChemComm Accepted Manuscript



Please do not adjust margins

Subsequent facile etherification of the chloride-substituted cyanine **2** with bis(pyrene) **1** was accomplished to afford the **BP-Cy** (Scheme 1a) in a 69 % yield. The **BP-Cy** was purified by column chromatography and the molecular structure was characterized by $^1$H NMR, MALDI-TOF, HR-Mass (See Supporting Information). The **BP-Cy** consists of a bis(pyrene)-extended hydrophobic cyanine core (shown green in Scheme 1b) with two hydrophilic carboxylic groups on one side (shown in red in Scheme 1b). Molecularly dissolved **BP-Cy** in $CH_2Cl_2$ shows a main absorption band at 790 nm reflecting the band gap of the S1 transition and an additional, less intense absorption band in the blue region that can be ascribed to a higher S2 transition (Figure S8).[27] Compared to the compound **2**, **BP-Cy** exhibits similar absorption and emission wavelength, whilst remarkably enhanced molar extinction coefficiency ($\varepsilon$ = 258000 $M^{-1}$ $cm^{-1}$) and fluorescence quantum yield (24.6 ± 0.3 %) in $CH_2Cl_2$ (Table S1), attributing to the introduction of large conjugated bis(pyrene).[28] Similarly, we studied that optical properties of **BP-Cy** in various solvents and the results suggested that **BP-Cy** (10 μM) dissolved in MeOH and DMSO in monomer state. When **BP-Cy** (10 μM) in DMSO was gradually changed to $H_2O$, **BP-Cy** transformed from monomeric to aggregated states (Figure S8a). The absorption band becomes broader with a shoulder peak at longer wavelength around 850 nm. Based on previous studies on perylene bisimides aggregates by Würthner's group.[27, 29] Meanwhile, the fluorescence of **BP-Cy** is dramatically quenched upon addition of water (Figure S8b).

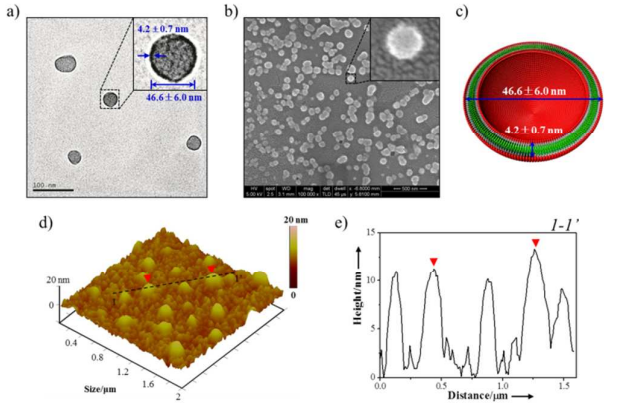


**Figure 1**. Morphologies of **BP-Cy** nanoaggregates. a) TEM images of **BP-Cy** vesicles with negative staining. The expansions indicate the thickness of the bilayer membrane and the diameter of the vesicle in each case. b) SEM images of **BP-Cy** nanoaggregates. c) Schematic space-filling model for the vesicle. d) AFM height images of **BP-Cy** nanoaggregates incubated on freshly cleaved mica surface at room temperature for 20 min. e) Cross-section analysis along the dark line **1-1'** in (d).

**BP-Cy** (10 μM) self-assembled into vesicular structures in DMSO/$H_2O$ mixed solution (v:v = 1:99), which was visualized by transmission electron microscope (TEM) (Figure 1a and S9). The diameter of these nanovesicles was 46.6 ± 6.0 nm and the thickness of the wall was 4.2 ± 0.7 nm, which corresponded to the length of two molecules packed in a head-to-head fashion as depicted in Figure 1c. Moreover, the **BP-Cy** aggregates were also observed by scanning electron microscope (SEM), which showed uniform nanoparticles in low magnification with a size of 59.9 ± 9.8 nm (Figure 1b). The morphology of **BP-Cy** aggregates *in situ* instead of that in the dry state were further observed by the atomic force microscope (AFM). The solution sample of **BP-Cy** aggregates were dropped cast on freshly cleaved mica surface and these flatten hollow nanovesicles with the height of 11.1 ± 2.3 nm and the diameter of 191.6 ± 33.2 nm were recorded (Figure 1d, e). The significant shape changes on a hard substrate further confirms the hollow structure of **BP-Cy** aggregates. In previous reports, the vesicular cyanine dye based aggregates can only be observed in the presence of surfactant by template-induced structural transition effect.[26] By conjugating large π-system of bis(pyrene) with strong hydrophobicity, we constructed cyanine based vesicular nanostructures through amphiphilic interactions without templates.

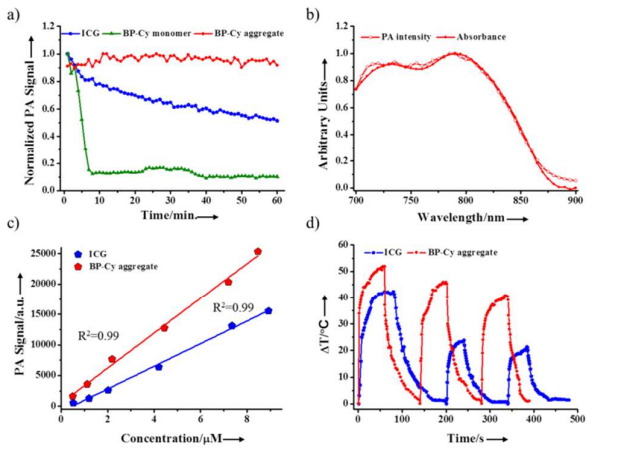


**Figure 2**. a) Photostability of ICG, **BP-Cy** monomer and **BP-Cy** aggregate under continuous illumination by 790 nm. b) The UV and PA spectra of **BP-Cy** aggregate in $H_2O$/DMSO (v/v = 99:1). c) The PA signal produced by **BP-Cy** aggregate (red line) and ICG (blue line) was observed to be linearly dependent on the molecular concentration ($R^2$=0.99). d) The heating/cooling curves of **BP-Cy** and ICG solution for continuous 3 times. The energy input from lasers was 490 mW at 790 nm.

The photostability of **BP-Cy** aggregates in water was studied. The UV-vis curves and PA signals of **BP-Cy** nanovesicles in water kept unchanged under continuous excitation at 790 nm by UV2600 spectrometer for 180 min (Figure S10a) or laser irradiation by Multi-Spectral Optoacoustic Tomography (MOST) for 60 min (Figure 2a), respectively. As a sharp contrast, the UV-vis spectrum and PA signals of **BP-Cy** monomers in THF dramatically decreased under the same conditions. The attributed the enhanced stability of **BP-Cy** aggregate to the well packed vesicular nanostructures constructed by amphiphilic interactions of **BP-Cy**, which provided the relative inert environment with reduced contact possibility with surroundings (oxygen, solvent and *etc.*) and hindered photo accelerated oxidation or dimerization degrade compare to small molecules in solution.[25b, 30] In addition, the **BP-Cy** was much more stable than ICG molecules in water, both of which are cationic polymethines and have the same length of the polymethine chains (Figure S10a and 2a). Furthermore, the chemical stability of **BP-Cy** were studied by temperature-dependent UV-Vis spectra and the results suggested higher thermostability of **BP-Cy** than ICG at the same condition (Figure S10b). The **BP-Cy** nanovesicles were also stable in various biological environments, *e.g.*, PBS with different pH (Figure S10c) and cell culture media (DMEM containing 10% fetal bovine serum and 1% penicillin-streptomycin) at 37 °C (Figure

ChemComm Accepted Manuscript



This journal is © The Royal Society of Chemistry 20xx

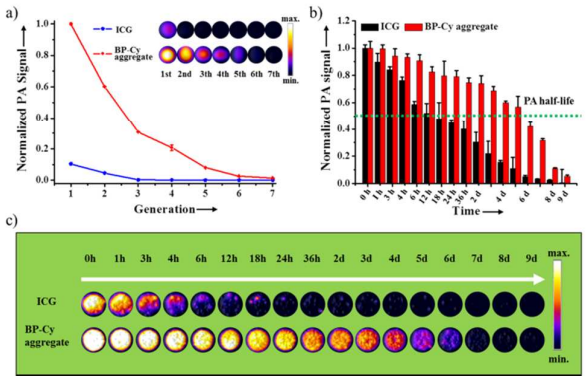


**Figure 3.** PA imaging of **BP-Cy** incubated in cells. a) The normalized PA signal of ICG (blue line) and **BP-Cy** aggregate (red line) cultured with MCF-7 breast cancer cells at 37 °C for 2 h and then subcultured for designated generations. b) The quantification of normalized PA signals from the phantom images c) of ICG (black column) and **BP-Cy** aggregate (red column) cultured MCF-7 breast cancer cells at 37 °C for 2 h with different intervals. The concentration of ICG and **BP-Cy** were 10 μM in the study. All data were repeated at least three times and expressed as mean ± SD (n=3). The phantom was imaged using a MOST 128 with 790 nm excitation pulse laser and reconstructed by ImageJ

S10d). The **BP-Cy** aggregates showed good biocompatibility *via* hemolysis assay (Table S2). The PA spectrum of **BP-Cy** aggregates showed peak at 790 nm, which was very similar with the UV-vis spectrum (Figure 2b), indicating the strong correlation between absorption and PA intensity.[22, 31]

The concentration-dependent PA intensity experiments of **BP-Cy** aggregates and ICG exhibited a good linear relationship ($R^2$ = 0.99) (Figure 2c). By calculating the slope, we found that **BP-Cy** aggregates showed 1.6 times higher PA intensity than that of ICG. To get the insight to enhanced PA intensity, we measured heating-cooling curves by using laser irradiation (490 mW, 790 nm). We calculated that the heat conversion efficiency (η)[32] of **BP-Cy** aggregates was 9.2 times higher than that of ICG (details see ESI). The aggregation-induced η enhancement unambiguously contributed the resulting PA signal. By monitoring three circles, we also observed that **BP-Cy** aggregates gave more significant temperature increase and lower loss of heating-generation capability compared to those of ICG (Figure 2d). The hollow nanovesicular structure with a thin bilayer and ease of expansion/compression maybe contribute to the higher photothermal conversion efficiency and PA signals of **BP-Cy** aggregates upon photo irradiation.[18]

Next, **BP-Cy** based nanovesicles were utilized as long-term cell tracking PA contrast agents by using human breast cancer MCF-7 cells as a model cell line.[33] The MCF-7 cells in Petri dishes at 100% confluence (~$10^6$ cells) were incubated with **BP-Cy** nanovesicles (10 μM based on **BP-Cy** molecules) and ICG (10 μM) for 2 h at 37 °C, respectively. The treated cells were referred as the 1st generation and utilized for PA imaging. At the same time, 50% of the cells in the completely filled Petri dish were transferred to a new dish with a fresh growth medium. The half-filled Petri dish after 36 h was referred to the 2nd generation. The cells were further incubated for another 36 h to the end of the 3rd generation. The processes were repeated to proceed to the 7th generation. PA imaging of **BP-Cy** nanovesicles incubated cells and ICG incubated cells at different generations were recorded by the MOST. Figure 3a showed that PA signals of MCF-7 cells at the first generation are 9.6 times higher than that of ICG treated group. The MCF-7 cells incubated with **BP-Cy** nanovesicles showed unambiguous PA signals even after five generations, whereas almost no PA signals were detectable in the ICG-incubated cells after only two generations (Figure 3a). The results clearly indicated the good cell tracking ability of **BP-Cy** nanovesicles over ICG dyes. The supramolecular **BP-Cy** nanovesicles are difficult to extrude out once they are internalized, combining with the high stability, which accounted for the remarkable cell tracking ability[34]. In addition, the cytotoxicity of **BP-Cy** nanovesicles was evaluated through CCK-8 assays to determine the cell viability of MCF-7 cells (see ESI for details). No significant cytotoxicity was observed with a concentration up to 20 μM under our experimental condition (Figure S12). We seeded MCF-7 cells into agar-based phantoms to study PA imaging effect of **BP-Cy** nanovesicles (Figures 3b and 3c). The time-dependent PA signals changes were evaluated by PA half-life, which was defined as the amount of time required for PA intensity to decrease to its half as measured at the beginning. The PA half-life of **BP-Cy** nanovesicles-treated phantoms was 5 days that was much longer than ICG treated groups (0.5 d), implying that long-term imaging is possible for further *in vivo* study.

To further evaluate the supramolecular **BP-Cy** nanovesicles as a long-term PA contrast agent *in vivo*, we carried out the PA imaging of breast tumor xenografted mice based on the **BP-Cy** nanovesicles (Figure 4a). The **BP-Cy** nanovesicles (20 μM, 200 μL) were firstly intravenously injected into mice *via* tail vein. The PA signals at tumor site were collected upon 700-850 nm excitations (Figure 4c). The PA signals were clearly observed in the tumor region after 2 h administration, which was gradually increased and reached a plateau at 12 h post-injection. After that, the PA signals decreased to a detectable level till 72 h. As a control, the PA signals of the ICG treated tumor xenografted mice only retained for 4 h with the maxima at 2 h. The sustained PA intensity in vivo could be ascribed to not only the ultrahigh stability of contrast agents but also somewhat enhanced accumulation and retention of **BP-Cy** nanoaggregates in tumor site (Figure 4b).[10d]

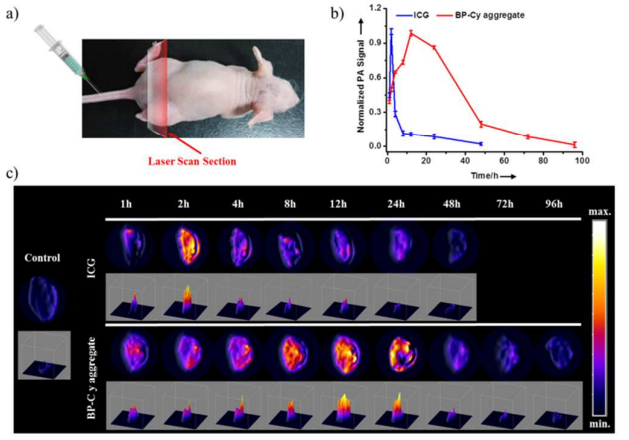


**Figure 4**. *In vivo* PA imaging of tumor-xenografted mice. a) *In vivo* model mice for PA imaging injected with ICG and **BP-Cy** aggregate (20 μM, 200 μL) via tail vein and detected under laser irradiation (700-850 nm). b) The quantification of normalized PA signals from the tumor injected with ICG corresponding PA images of tumors.

ChemComm Accepted Manuscript

In summary, we have constructed a supramolecular NIR absorbing cyanine dye based aggregates as a long-term PA imaging contrast agent. Our results demonstrated that supramolecular strategy can effectively improve the photophysical properties of building blocks, which are highly demanded for bottom-up fabrication of functional materials and devices. We believed that this hollow nanostructure can be potentially employed as a platform for delivery of various bioactive molecules for extensive biomedical applications.

We thank the National Basic Research Program of China (973 Program, 2013CB932701), National Natural Science Foundation of China (21374026, 51473188, 21304023, and 51303036) and Beijing Natural Science Foundation (2132053) and the 100-Talent Program of the Chinese Academy of Science (Y2462911ZX) for funding support.

## Notes and references

1 a) M. Sun, H.-Y. Zhang, B.-W. Liu, Y. Liu, *Macromolecules* **2013**, *46*, 4268-4275; b) Y. Chen, Y. Liu, *Chem. Soc. Rev.***2010**, *39*, 495-505.

2 a) P. A. Korevaar, S. J. George, A. J. Markvoort, M. M. Smulders, P. A. Hilbers, A. P. Schenning, T. F. De Greef, E. W. Meijer, *Nature* **2012**, *481*, 492-497; b) S. Prasanthkumar, S. Ghosh, V. C. Nair, A. Saeki, S. Seki, A. Ajayaghosh, *Angew. Chem. Int. Ed.* **2015**, *54*, 946-950; c) D.-S. Guo, Y. Liu, *Acc. Chem. Res.* **2014**, *47*, 1925-1934; d) J. Boekhoven, C. M. Rubert Pérez, S. Sur, A. Worthy, S. I. Stupp, *Angew. Chem. Int. Ed.* **2013**, *52*, 12077-12080; e) D. Zhang, Y.-X. Zhao, Z.-Y. Qiao, U. Mayerhöffer, P. Spenst, X.-J. Li, F. Würthner, H. Wang, *Bioconjugate Chem.* **2014**, *25*, 2021-2029.

3 a) Q. Wang, J. L. Mynar, M. Yoshida, E. Lee, M. Lee, K. Okuro, K. Kinbara, T. Aida, *Nature* **2010**, *463*, 339-343; b) Z. Huang, L. Yang, Y. Liu, Z. Wang, O. A. Scherman, X. Zhang, *Angew. Chem. Int. Ed.* **2014**, *53*, 5351-5355; c) F. Wang, Z. Liu, B. Wang, L. Feng, L. Liu, F. Lv, Y. Wang, S. Wang, *Angew. Chem. Int. Ed.* **2014**, *53*, 424-428.

4 a) X. Liu, M. Jiang, *Angew. Chem. Int. Ed.* **2006**, *45*, 3846-3850; b) W. Cao, X. Zhang, X. Miao, Z. Yang, H. Xu, *Angew. Chem. Int. Ed.* **2013**, *52*, 6233-6237; c) J. Chen, C. Yu, Z. Shi, S. Yu, Z. Lu, W. Jiang, M. Zhang, W. He, Y. Zhou, D. Yan, *Angew. Chem. Int. Ed.* **2015**, *54*, 1-6.

5 a) M. Schulze, A. Steffen, F. Würthner, *Angew. Chem. Int. Ed.* **2015**, *54*, 1570-1573; b) J. H. Lee, K. J. Chen, S. H. Noh, M. A. Garcia, H. Wang, H. Jeong, B. J. Kong, D. B. Stout, J. Cheon, H. R. Tseng, *Angew. Chem. Int. Ed.* **2013**, *52*, 4384-4388.

6 L.-L. Li, J.-H. Xu, G.-B. Qi, X. Zhao, F. Yu, H. Wang, *ACS Nano* **2014**, *8*, 4975-4983.

7 T. Sun, Y. S. Zhang, B. Pang, D. C. Hyun, M. Yang, Y. Xia, *Angew. Chem. Int. Ed.* **2014**, *53*, 12320-12364.

8 a) A. Thayil, T. Watanabe, A. Jesacher, T. Wilson, S. Srinivas, M. Booth, *J. Biomed. Opt.* **2011**, *16*, 046018; b) Y. Adam, A. Mizrahi, *J. Neurosci.* **2011**, *31*, 7967-7973.

9 J. T. Trachtenberg, r. E. Chen, G. W. Knott, G. Feng, J. R. Sanes, E. Welker, K. Svoboda, *Nature* **2002**, *420*, 788-794.

10 a) J. F. Lovell, C. S. Jin, E. Huynh, H. Jin, C. Kim, J. L. Rubinstein, W. C. W. Chan, W. Cao, L. V. Wang, G. Zheng, *Nat. Mater.* **2011**, *10*, 324-332; b) G. D. Moon, S.-W. Choi, X. Cai, W. Li, E. C. Cho, U. Jeong, L. V. Wang, Y. Xia, *J. Am. Chem. Soc.* **2011**, *133*, 4762-4765; c) K. Pu, A. J. Shuhendler, J. V. Jokerst, J. Mei, S. S. Gambhir, Z. Bao, J. Rao, *Nat. Nanotechnol.* **2014**, *9*, 233-239; d) A. de la Zerda, Z. Liu, S. Bodapati, R. Teed, S. Vaithilingam, B. T. Khuri-Yakub, X. Chen, H. Dai, S. S. Gambhir, *Nano Lett.* **2010**, *10*, 2168-2172.

11 K. Welsher, Z. Liu, S. P. Sherlock, J. T. Robinson, Z. Chen, D. Daranciang, H. Dai, *Nat. Nanotechnol.* **2009**, *4*, 773-780.

12 E. V. Shashkov, M. Everts, E. I. Galanzha, V. P. Zharov, *Nano Lett.* **2008**, *8*, 3953-3958.

13 G. Ku, M. Zhou, S. Song, Q. Huang, J. Hazle, C. Li, *ACS Nano* **2012**, *6*, 7489-7496.

14 W. Wu, W. Driessen, X. Jiang, *J. Am. Chem. Soc.* **2014**, *136*, 3145-3155.

15 T. Temma, S. Onoe, K. Kanazaki, M. Ono, H. Saji, *J. Biomed. Opt.* **2014**, *19*, 090501.

16 H. Y. Ahn, S. Yao, X. Wang, K. D. Belfield, *ACS Appl. Mater. Interfaces* **2012**, *4*, 2847-2854.

17 X. Wang, G. Ku, M. A. Wegiel, D. J. Bornhop, G. Stoica, L. V. Wang, *Opt. Lett.* **2004**, *29*, 730-732.

18 E. Huynh, C. S. Jin, B. C. Wilson, G. Zheng, *Bioconjugate Chem.* **2014**, *25*, 796-801.

19 a) C. D. Geddes, H. Cao, J. R. Lakowicz, *Spectrochim. Acta A* **2003**, *59*, 2611-2617; b) X. Chen, X. Peng, A. Cui, B. Wang, L. Wang, R. Zhang, *J. Photochem. Photobiol. A* **2006**, *181*, 79-85.

20 D. M. Liu, R. C. Huxford, W. B. Lin, *Angew. Chem. Int. Ed.* **2011**, *50*, 3696-3700.

21 F. Song, X. Peng, E. Lu, R. Zhang, X. Chen, B. Song, *J. Photochem. Photobiol. A* **2004**, *168*, 53-57.

22 H. Wang, C. Liu, X. Gong, D. Hu, R. Lin, Z. Sheng, C. Zheng, M. Yan, J. Chen, L. Cai, L. Song, *Nanoscale* **2014**, *6*, 14270-14279.

23 a) L. Wang, L.-l. Li, Y.-s. Fan, H. Wang, *Adv. Mater.* **2013**, *25*, 3888-3898; b) P.-P. Yang, Y. Yang, Y.-J. Gao, Y. Wang, J.-C. Zhang, Y.-X. Lin, L. Dai, J. Li, L. Wang, H. Wang, *Adv. Optical Mater.* **2014**, DOI: 10.1002/adom.201400522; c) F. P. Gao, Y. X. Lin, L. L. Li, Y. Liu, U. Mayerhoffer, P. Spenst, J. G. Su, J. Y. Li, F. Würthner, H. Wang, *Biomaterials* **2014**, *35*, 1004-1014; d) J. H. Xu, F. P. Gao, X. F. Liu, Q. Zeng, S. S. Guo, Z. Y. Tang, X. Z. Zhao, H. Wang, *Chem. Commun.* **2013**, *49*, 4462-4464.

24 a) L. Wang, W. Li, J. Lu, Y.-X. Zhao, G. Fan, J.-P. Zhang, H. Wang, *J. Phys. Chem. C* **2013**, *117*, 26811-26820; b) W. Li, L. Wang, J.-P. Zhang, H. Wang, *J. Mater. Chem. C* **2014**, *2*, 1887-1892.

25 a) D. M. Eisele, J. Knoester, S. Kirstein, J. P. Rabe, D. A. Vanden Bout, *Nat. Nanotechnol.* **2009**, *4*, 658-663; b) H. v Berlepsch, C. Bottcher, *Langmuir* **2013**, *29*, 4948-4958; c) H. Yao, Y. Kagoshima, S.-i. Kitamura, T. Isohashi, Y. Ozawa, K. Kimura, *Langmuir* **2003**, *19*, 8882-8887; d) H. Yao, T. Isohashi, K. Kimura, *Chem. Phys. Lett.* **2004**, *396*, 316-322.

26 E. Barni, P. Savarino, E. Pelizzetti, G. Rothenberger, *Helv. Chim. Acta* **1981**, *64*, 1943-1948.

27 X. Zhang, D. Gorl, V. Stepanenko, F. Würthner, *Angew. Chem. Int. Ed.* **2014**, *53*, 1270-1274.

28 a) K. Li, W. Qin, D. Ding, N. Tomczak, J. Geng, R. Liu, J. Liu, X. Zhang, H. Liu, B. Liu, B. Z. Tang, *Sci. Rep.* **2013**, *3*, 1150; b) N. S. James, Y. Chen, P. Joshi, T. Y. Ohulchanskyy, M. Ethirajan, M. Henary, L. Strekowsk, R. K. Pandey, *Theranostics* **2013**, *3*, 692-702.

29 T. E. Kaiser, H. Wang, V. Stepanenko, F. Würthner, *Angew. Chem. Int. Ed.* **2007**, *46*, 5541-5544.

30 E. I. Altınoğlu, T. J. Russin, J. M. Kaiser, B. M. Barth, P. C. Eklund, M. Kester, J. H. Adair, *ACS Nano* **2008**, *2*, 2075-2084.

31 C. J. Ho, G. Balasundaram, W. Driessen, R. McLaren, C. L. Wong, U. S. Dinish, A. B. Attia, V. Ntziachristos, M. Olivo, *Sci Rep* **2014**, *4*, 5342.

32 Q. Tian, F. Jiang, R. Zou, Q. Liu, Z. Chen, M. Zhu, S. Yang, J. Wang, J. Wang, J. Hu, *ACS Nano* **2011**, *5*, 9761-9771.

33 A. Dragulescu-Andrasi, S. R. Kothapalli, G. A. Tikhomirov, J. Rao, S. S. Gambhir, *J. Am. Chem. Soc.* **2013**, *135*, 11015-11022.

34 Y. Yu, C. Feng, Y. Hong, J. Liu, S. Chen, K. M. Ng, K. Q. Luo, B. Z. Tang, *Adv. Mater.* **2011**, *23*, 3298-3302.

ChemComm Accepted Manuscript



This journal is © The Royal Society of Chemistry 20xx